Journal of Solid State Chemistry 188 (2012) 100–104

Contents lists available at SciVerse ScienceDirect

Journal of Solid State Chemistry

journal homepage: www.elsevier.com/locate/jssc

Highly ordered magnetic mesoporous silicas for effective elimination of carbon monoxide

Jiho Lee [a,b], Jeong Ho Chang [a,*]

[a] Korea Institute of Ceramic Engineering and Technology, Seoul 153-801, South Korea
[b] Department of Chemistry, Inha University, Incheon 402-751, South Korea

ARTICLE INFO

Article history:
Received 5 December 2011
Received in revised form
20 January 2012
Accepted 23 January 2012
Available online 30 January 2012

Keywords:
Fe nanoparticles
Mesoporous Silicas
Carbon monoxide
Elimination
Catalysts

ABSTRACT

Catalysts based on crystalline nanoparticles of Fe metal supported on mesoporous silica have been developed. The synthetic process involves hydrogen reduction processing for high abundant Fe metal nanoparticles within the mesopores, in which impregnated Fe salt in the inner nanopores of mesoporous silica is thermally treated under hydrogen at 500 °C. Detailed characterization was achieved by XRD, XPS, BET, and HR-TEM techniques. The catalytic efficiency was demonstrated as a function of the used amounts and reaction time. The results show that more than 90% of the carbon monoxide was eliminated at room temperature during a period 80 min with 0.5 g of catalyst.

1. Introduction

Carbon monoxide (CO) is tasteless, non-irritating, and colorless but poisonous to humans and a major air pollutant [1]. CO is emitted from vehicles (about 50–60% of total emission), industrial processes, and other processes [2]. Its presence even in trace amounts can cause serious environmental and health problems. Consequently, the effective elimination of CO is to an important issue. There have recently been numerous studies on the control of CO using catalytic approaches in order to improve the low temperature activity, stability, selectivity, and cost of existing methods [3,4]. In particular, heterogeneous catalysts are important for the successful elimination of CO. These catalysts are mainly applied to elimination of CO from automobiles as well as chemical production and processing in industries [5–8]. To date, noble metal supported catalysts have played important roles in practical application. However, due to high cost and limited resources, these precious metals are not a practical option for replacement.

In efforts to address these disadvantages, research on metal supported mesoporous silica catalysts has recently been carried out. Mesoporous silica (MS) has a large surface, tunable porosity, uniform pore size distribution, and high thermal stability [9]. For this reason, MS can potentially be exploited in a wide variety of applications such as biological immobilization, separation, heterogeneous catalysis, and sensor, and so on [10–17]. Several representative reports have described the use of MS in CO elimination, as follows: Huang et al. reported low Pt loading (0.5–1.0%) catalysts supported on a series of FSM-type MS materials for preferential oxidation of CO [18]. Joo et al. designed thermally stable Pt coated MS catalysts for CO oxidation [19]. Chi et al. prepared Au nanoparticle embedded within MS particles for CO oxidation [20].

In this work, we focused on the development of a MS based heterogeneous catalyst using iron nanoparticles for effective CO elimination. Fe nanoparticles are of technological importance as catalytic materials as well as in applications such as gas sensors, coating materials, bioseparation, and biosensing [21–23]. Fe nanoparticle-based catalysts have been identified as candidates for cheap and efficient catalysts. Our strategy for the synthesis of a highly abundant Fe embedded MS catalyst adopts hydrogen reduction at high temperature. This process is particularly useful in homogeneous formation of Fe nanoparticles from Fe ions within MS channels (Scheme 1). We are tried to demonstrate for novel approach with ordered magnetic mesoporous silica (MS) materials, in which they have the high surface areas by the homogeneous nanopores and channels. We propose a novel synthesis of highly ordered magnetic mesoporous silica materials with a high abundance and a homogeneous dispersion of iron nanoparticles within the mesopores by the hydrogen reduction after incorporation of ferrous ion to prevent the clogging of mesopores. The novel hydrogen reduction process for homogeneous development of

* Corresponding author. Fax: +82 2 3238 7811.
E-mail address: jhchang@kicet.re.kr (J. Ho Chang).

0022-4596/$ - see front matter © 2012 Elsevier Inc. All rights reserved.
doi:10.1016/j.jssc.2012.01.050

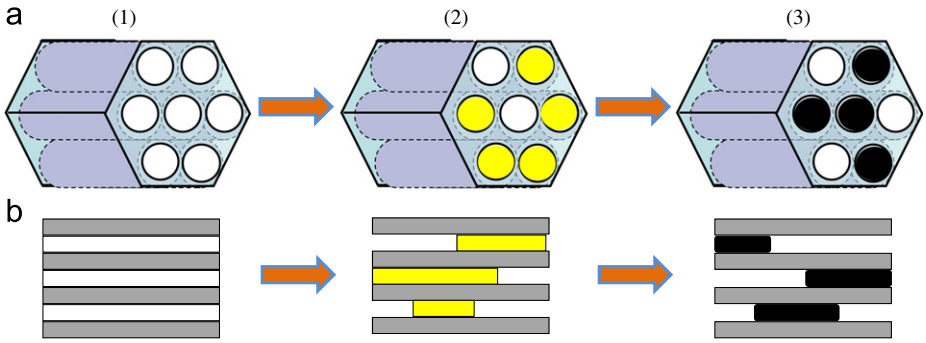

Scheme 1. Preparation strategy of FeMS composites ((a) transverse section; (b) longitudinal section). (1) MS, (2) Fe^{2+} ions introduced into the ordered MS channels; (3) hydrogen reduction at 400 °C.

metal nanoparticles from metal ions opens new opportunities for further synthesis of Fe materials in confined environments and their use in catalytic applications.

2. Materials and methods

2.1. Materials

Tri-block copolymer Pluronic P123(M_{av} = ~5,800, $PEO_{20}PPO_{70}PEO_{20}$) was purchased from BASF, and tetraethyl orthosilicate (TEOS, 98%, reagent grade), hydrochloride (HCl, 37%, A.C.S reagent) and iron(II) chloride tetrahydrate ($FeCl_2 \cdot 4H_2O$, 99%, ReagentPlus®) were purchased from Sigma–Aldrich Co. All chemicals were used as received without any further purification.

2.2. Synthesis of mesoporous silicas (MS)

The synthesis of MS was carried out according to the procedure in our previous report [24]. Tri-block copolymer Pluronic P123 was dispersed in an aqueous hydrochloric acid solution ($1 < pH < 2$) under vigorous stirring at 40 °C. A clear solution was obtained indicating a complete dissolution of the surfactant. TEOS as a silica source was added dropwisely to the solution at 40 °C. Gelation and ageing were carried out at 40 °C for 8 h, followed by heating at 120 °C for 8 h in a still bomb. The solid was filtered, washed several times with distilled water, and dried at room temperature. The organic template was removed by calcination in air at 550 °C (heating rate 9.2 °C/min) for 8 h.

2.3. Synthesis of Fe-impregnated MS (FeMS)

A wet impregnation method was employed to prepare the Fe-impregnated MS composites. MS was dispersed in distilled water at room temperature under stirring. Iron chloride was dissolved in 250 mL of distilled water. This solution was added via incipient wetness impregnation to 5 g of MS and subsequently stirred for 1 h at room temperature. After vacuum drying, the yellow powder was collected and heated under a hydrogen atmosphere at 400 °C for 2 h.

2.4. Instrumental analyses and CO elimination detection

Small-angle X-ray diffraction patterns were obtained on a Rigaku DMAX-2500 diffractometer using Cu$K\alpha$1 radiation. The samples were scanned in 2θ range 0.5–4° with a scanning speed of 2° min^{-1}. Wide-angle X-ray diffraction patterns were recorded using a Rigaku DMAX-2500 Instrument with Cu$K\alpha$1 radiation. The samples were scanned in the 2θ range from 20 to 90° with a scanning speed of 2° min^{-1}. Diffraction peaks were compared with the calculated database results reported in the Joint Committee on Powder Diffraction Standards (JCPDS). X-ray photoelectron spectroscopy (XPS) was measured with a Thermo VG SIGMA PROBE. N_2 adsorption-desorption isotherms was obtained with a Bel-Japan Belsorp-mini II. The Brunauer–Emmett–Teller (BET) method was utilized to calculate the surface areas. Pore size distribution curves were obtained from the desorption branch calculated by the Barrett–Joyner–Halenda (BJH) method. The morphological and structural details of the material were also studied by field emission scanning electron microscopy (FE-SEM) and high resolution transmission electron microscopy (HR-TEM). FE-SEM investigations were carried out with a JEOL JSM-6700F instrument using 10 kV accelerating voltage. HR-TEM was carried out on a JEOL JEM-4010 electron microscope operated at 400 kV. Inductively coupled plasma optical emission spectrometry (ICP-OES) was carried out on a Perkin Elmer instrument. Furthermore, the detection of CO elimination was achieved by a FT-IR with a JASCO FTIR-460 spectrometer (resolution 4 cm^{-1}, integration 20 times) with measurements performed at room temperature. 0.5 g of the Fe-MS catalyst was used in a vial. A FT-IR gas cell with KBr windows was filled with CO gas (50 mL), and the IR gas cell was then connected to the vial. The FT-IR spectrum was obtained at every 10 min at room temperature.

3. Results and discussion

Fig. 1 shows FE-SEM images presenting the morphologies of the as-prepared MS and reduced FeMS. The as-prepared MS exhibits a typical cylinder-like morphology and a regular array of uniform channels (Fig. 1(a)). As shown in Fig. 1(b), the morphology and straight pores were changed after hydrogen reduction treatment for 2 h at 400 °C. The walls of the MS were randomly etched by penetration of impregnated Fe ions. Pores formed at the outer surface and the pore diameter was in a range of 10–20 nm.

Fig. 2 shows N_2 adsorption-desorption isotherms of MS and FeMS. The isotherms were identified as type IV and exhibit significant hysteresis loops with capillary condensation at relative pressure of around 0.66–0.90 and 0.70–0.97, respectively. In addition, according to the Kelvin equation, the FeMS has a larger pore diameter because hysteresis occurs at higher relative pressures (P/P_0). The detailed structural parameters of FeMS materials are shown in Table 1. FeMS materials show a relatively broad pore size distribution, which implies the ordered mesoporous structures of FeMS are deteriorated somewhat due to Fe addition. It is speculated that the Fe precursor decomposed into iron oxide upon heating and was further reduced by H_2 gas to Fe particles at high temperatures.

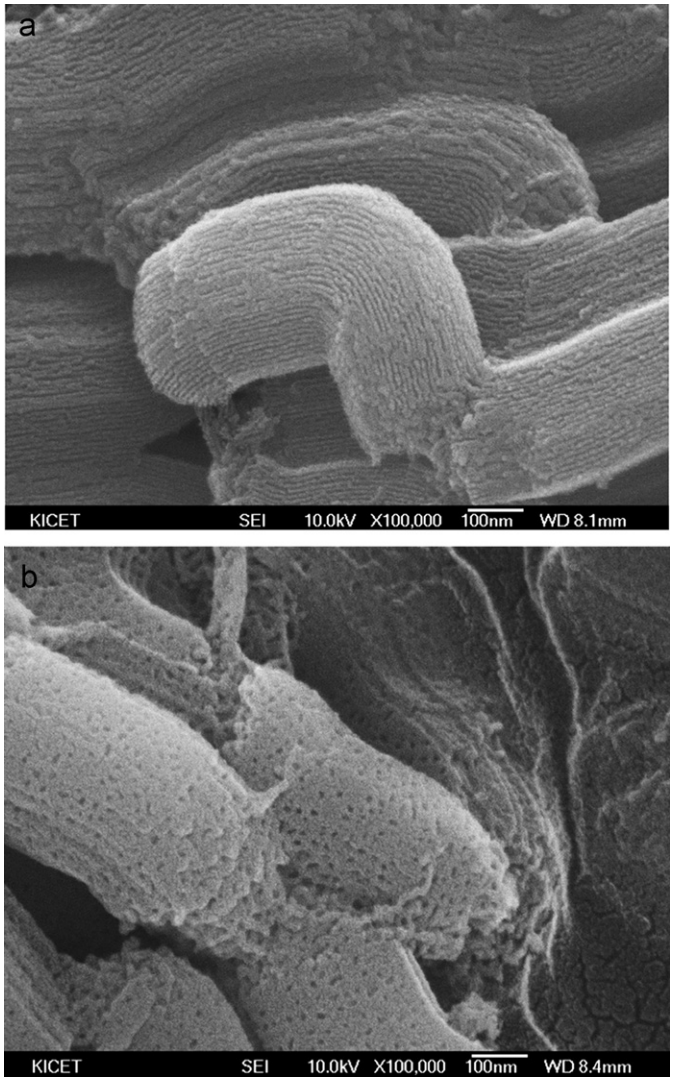

Fig. 1. FE-SEM images of (a) MS, and (b) FeMS.

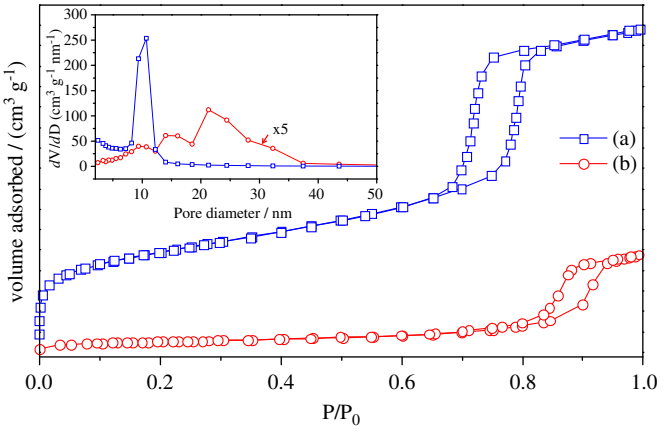

Fig. 2. N_2 adsorption/desorption isotherms of (a) MS, and (b) FeMS (insets are their pore-size distributions).

The small-angle X-ray diffraction patterns of MS and FeMS are shown in Fig. 3(A). Typically, the small-angle XRD pattern shows evidence of three reflection peaks at 2θ values of 0.5°–3°, (1 0 0), (1 1 0), and (2 0 0), corresponding to a highly ordered hexagonal mesoporous silica framework. The XRD pattern of FeMS is the same as that of MS, and the long-range order of the MS framework was well retained after the reduction process. The shift of diffraction peaks indicated that the mesopores are filled with iron nanoparticles. Fig. 3(A) shows wide-angle XRD patterns of mesoporous silica and iron-impregnated mesoporous silica. A broad peak centered at 22.2° of 2θ was observed for all samples, indicating that the pore walls of MS and FeMS are amorphous. This result was in accordance with the low-angle patterns. The d-spacing of FeMS is 0.203, 0.143, and 0.117 nm, which are consistent with the (1 1 0), (2 0 0), and (2 1 1) diffraction of body-centered cubic (bcc) α-Fe (JCPDS card no. 06-0696).

The XPS results of the Fe nanoparticles are shown in Fig. 3(B). The major characteristic peaks of FeMS are seen at 710.6 eV,

Table 1
Physicochemical properties of MS and FeMS materials.

Specimens	S_{BET} (m^2/g)[a]	V_{Total} (m^3/g)[b]	D (nm)[c]
MS	761.1	1.42	9.44
FeMS	91.09	0.366	17.7

[a] S_{BET}: specific surface area computed using BET equation in a relative pressure range of 0.2–0.3.
[b] V_{Total}: total pore volume is estimated at a relative pressure $P/P0=0.99$.
[c] D: adsorption average pore width determined from BET method.

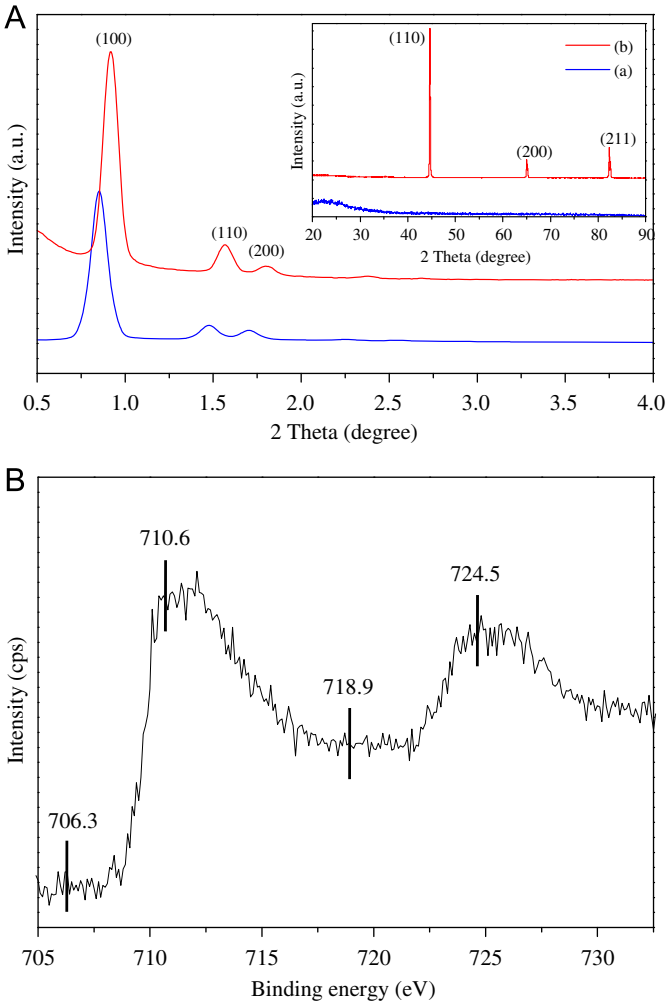

Fig. 3. (A) (a) Small-angle XRD patterns of MS templates and (b) FeMS (comparative wide-angle XRD patterns is inserted) (B) XPS spectra of Fe_{2p} in the FeMS composites.

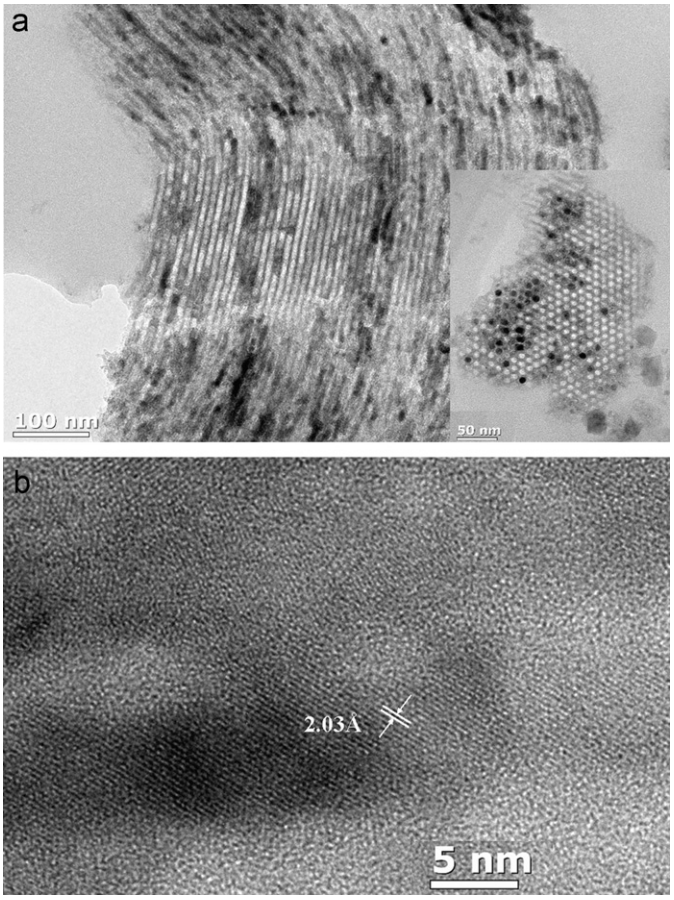

Fig. 4. HR-TEM images of Fe nanoparticles within the ordered MS channels. (a) cross-section view of FeMS, and (b) Fe nanoparticles in FeMS.

718.9 eV and 724.5 eV corresponding to Fe($2p_{3/2}$), and shake-up satellites $2p_{3/2}$ and $2p_{1/2}$, respectively [25]. Moreover, a small shoulder is seen at around 706.3 eV, reflecting the $2p_{3/2}$ peaks of zero-valent iron (Fe^0). Based on the results of wide-angle XRD and XPS, we concluded that the iron nanoparticles have a zero-valent iron (Fe^0) while it interacts with the silica wall (i.e., Fe–O–Si).

Fig. 4 shows the structure and dimensions of Fe nanoparticles within the mesopores by HR-TEM including a cross-sectional view. At a reduction temperatures of 400 °C, the FeMS retains a hexagonal structure with 7.8 nm average pore size. Fig. 4(b) shows a HR-TEM image with high magnification of Fe nanoparticles. This image displays perfect arrangement of the atomic layers, where the lattice plane distance was 2.03 Å. This result is consistent with the [1 1 0] plane of α-Fe.

The catalytic property of the FeMS was evaluated by an IR gas cell (with KBr windows, capacity of 50 cm^3) containing CO gas at ambient temperature. Two major bands are seen at 2,117 cm^{-1} and 2,171 cm^{-1}, corresponding to the ν_{co} stretching (Fig. 5(a)). Furthermore, the intensity of the gaseous CO peaks decreases gradually as a function of time. The catalytic behavior is also explored as a function of the used amount of FeMS (Fig. 5(b)). The previous reports by conventional process were not shown the homogeneous development of metal or metal oxides nanoparticles within the ordered mesopores, in which the catalytic efficiency was not much due to the low reactivity [26]. Furthermore, the negligible catalytic efficiency was observed at room temperature in many reports [27,28]. However, a result of the work showed that more than 90% gaseous CO elimination was attained with 0.50 g of FeMS for 80 min.

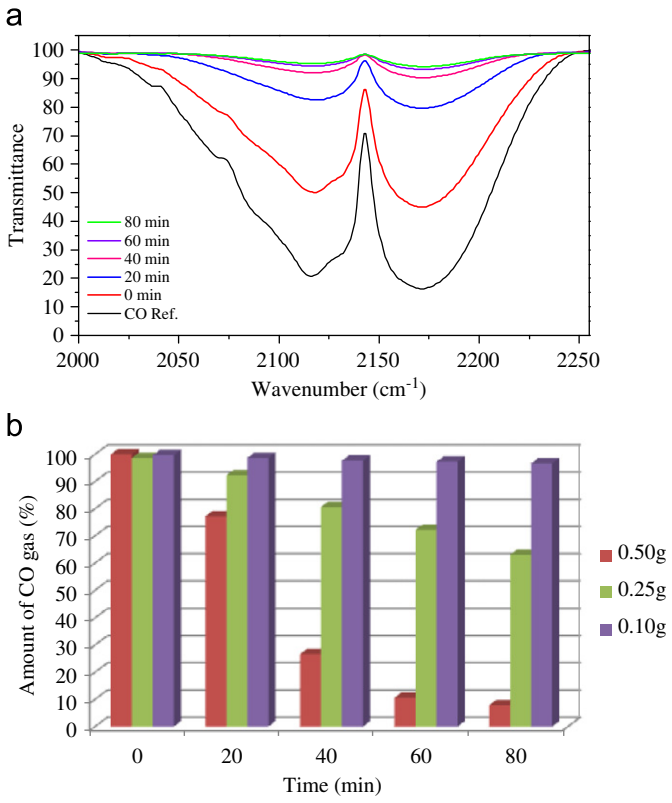

Fig. 5. (a) FT-IR spectra of FeMS for elimination of gaseous CO as a function of reaction time with 0.5 g catalysts, and (b) elimination efficiency with various catalyst weight at ambient temperature.

4. Conclusion

A highly abundant Fe nanoparticle embedded MS catalyst was synthesized by a novel hydrogen reduction process and demonstrated CO elimination at room temperature. The synthetic process involved impregnated Fe salt on the inner nanopores of mesoporous silica thermally treated under hydrogen at 500 °C. Based on detailed characterization including XRD, XPS, BET, and HR-TEM analyses, it was determined that the magnetic Fe nanoparticles were transformed to α-Fe metal from Fe ions. The catalytic efficiency was demonstrated as a function of the used amounts and reaction time. The results indicate that more than 90% of the carbon monoxide was eliminated at room temperature during a period of 80 min with 0.5 g of catalyst. This preliminary study could lead to the facile design and construction of MS based heterogeneous catalysts including nanoparticles or nanorods, which may overcome the disadvantages of conventional processes, such as low yields and difficult synthetic processing.

Acknowledgment

This work was supported by grant from the Fundamental R&D Program for Core Technology of Materials funded by the Ministry of Knowledge Economy, Republic of Korea.

References

[1] T. Meredith, A. Vale, Br. Med. J. 296 (1988) 77.
[2] A.F. Sedda, G. Rossi, Forensic Sci. Int. 164 (2006) 164.
[3] X. Xie, Y. Li, Z.Q. Liu, M. Haruta, W. Shen, Nature 458 (2009) 746.
[4] M. Date, M. Okumura, S. Tsubota, M. Haruta, Angew. Chem. Int. 43 (2004) 2129.

[5] G. Pattrick, E. Van der Lingen, C. Corti, R. Holliday, D. Thompson, Top. Catal. 30 (2004) 273.
[6] S. Alayoglu, A.U. Nilekar, M. Mavrikakis, B. Eichhorn, Nat. Mater. 7 (2008) 333.
[7] M.A. Barteau, Top. Catal. 22 (2003) 3.
[8] G.J. Hutchings, Catal. Lett. 75 (2001) 1.
[9] S.Y. Lee, J. Lee, J.H. Chang, J.H. Lee, BMB Rep. 44 (2011) 77.
[10] T. Itoh, R. Ishii, T. Ebina, T. Hanaoka, T. Ikeda, Y. Urabe, Y. Fukushima, F. Mizukami, Biotechnol. Bioeng. 97 (2007) 200.
[11] R.M. Blanco, P. Terreros, M. Fernandez-Perez, C. Otero, G. Diaz-Gonzalez, J. Mol. Catal. B 30 (2004) 83.
[12] H. Kyung Choi, J.H. Chang, I. Hwan, Ko, J. Hyung Lee, B. Yong Jeong, J. Hee Kim, J.Bae Kim, J. Solid State Chem. 184 (2011) 805.
[13] B.L. Newalkar, N.V. Choudary, P. Kumar, S. Komarneni, T.S.G. Bhat, Chem. Mater. 14 (2002) 304.
[14] S. Kim, S.U. Son, S.I. Lee, T. Hyeon, Y.K. Chung, J. Am. Chem. Soc. 122 (2000) 1550.
[15] C.M. Crudden, M. Sateesh, R. Lewis, J. Am. Chem. Soc. 127 (2005) 10045.
[16] I.I. Slowing, B.G. Trewyn, S. Giri, V.S.-Y. Lin, Adv. Funct. Mater. 17 (2007) 1225.
[17] T. Wagner, T. Waitz, J. Roggenbuck, M. Fröba, C.-D. Kohl, M. Tiemann, Thin Solid Films 515 (2007) 8360.
[18] S. Huang, K. Hara, Y. Okubo, M. Yanagi, H. Nambu, A. Fukuoka, Appl. Catal., A 365 (2009) 268.
[19] S.H. Joo, J.Y. Park, C. Tsung, Y. Yamada, P. Yang, G.A. Somorjai, Nat. Mater. 8 (2009) 126.
[20] Y. Chi, H. Lin, C. Mou, Appl. Catal., A 284 (2005) 199.
[21] Y. Tang, S. Cao, Y. Chen, T. Lu, Y. Zhou, L. Lu, J. Bao, Appl. Surf. Sci. 256 (2010) 4196.
[22] A. Tomescu, R. Alexandrescu, I. Morjan, F. Dumitrache, L. Gavrila-Florescu, R. Birjega, I. Soare, G. Prodan, Z. Bastl, A. Galikova, J. Mater. Sci. 42 (2007) 1838.
[23] Q.A. Pankhurst, J. Connolly, S. Jones, J. Dobson, J. Phys. D 36 (2003) R167.
[24] J.H. Chang, K.J. Kim, Y.K. Shin, J. Liu, Chem. Lett. 33 (2004) 1204.
[25] Y.P. Sun, X.Q. Li, W.X. Zhang, H.P. Wang, Colloids Surf., A 308 (2007) 60.
[26] Y. Li, Y. Guan, R.A. Santen, P.J. Kooyman, I. Dugulan, C. Li, J.M. Hensen, J. Phys. Chem. C 113 (2009) 21831.
[27] A. Fukuoka, J. Kimura, T. Oshio, Y. Sakamoto, M. Ichikawa, J. Am. Chem. Soc. 129 (2007) 10120.
[28] S. Huang, K. Hara, Y. Okubo, M. Yanagi, H. Nambu, A. Fukuoka, Appl. Catal., A 365 (2009) 268.